PERGAMON

Atmospheric Environment 35 (2001) 3967–3977

ATMOSPHERIC ENVIRONMENT

www.elsevier.com/locate/atmosenv

Direct radiative forcing and atmospheric absorption by boundary layer aerosols in the southeastern US: model estimates on the basis of new observations

Shaocai Yu[a,*], Charles S. Zender[b], V.K. Saxena[c]

[a] *Nicholas School of the Environment, Duke University, Durham, NC 27708, USA*
[b] *Department of Earth System Science, University of California, Irvine CA 92697-3100, USA*
[c] *Department of Marine, Earth and Atmospheric Sciences, North Carolina State University, Box 8208, Raleigh, NC 27695-8208, USA*

Received 30 September 2000; accepted 28 February 2001

Abstract

In an effort to reduce uncertainties in the quantification of aerosol direct radiative forcing (ADRF) in the southeastern United States (US), a field column experiment was conducted to measure aerosol radiative properties and effects at Mt. Mitchell, North Carolina, and at an adjacent valley site. The experimental period was from June 1995 to mid-December 1995. The aerosol optical properties (single scattering albedo and asymmetry factor) needed to compute ADRF were obtained on the basis of a procedure involving a Mie code and a radiative transfer code in conjunction with the retrieved aerosol size distribution, aerosol optical depth, and diffuse-to-direct solar irradiance ratio. The regional values of ADRF at the surface and top of atmosphere (TOA), and atmospheric aerosol absorption are derived using the obtained aerosol optical properties as inputs to the column radiation model (CRM) of the community climate model (CCM3). The cloud-free instantaneous TOA ADRFs for highly polluted (HP), marine (M) and continental (C) air masses range from 20.3 to -24.8, 1.3 to -10.4, and 1.9 to $-13.4\,W\,m^{-2}$, respectively. The mean cloud-free 24-h ADRFs at the TOA (at the surface) for HP, M, and C air masses are estimated to be -8 ± 4 (-33 ± 16), -7 ± 4 (-13 ± 8), and -0.14 ± 0.05 (-8 ± 3) $W\,m^{-2}$, respectively. On the assumption that the fractional coverage of clouds is 0.61, the annual mean ADRFs at the TOA and the surface are -2 ± 1, and $-7 \pm 2\,W\,m^{-2}$, respectively. This also implies that aerosols currently heat the atmosphere over the southeastern US by $5 \pm 3\,W\,m^{-2}$ on annual timescales due to the aerosol absorption in the troposphere.

Keywords: Aerosol radiative forcing; Column radiation model; Southeastern US; Observation; Aerosol absorption

1. Introduction

Eastern China, south central Europe and the eastern United States (US) are regions where the radiative forcing of anthropogenic sulfate aerosols supersedes that of anthropogenic greenhouse gases, manifesting itself in terms of cooling of the surface-air temperature (IPCC, 1995; Kiehl and Briegleb, 1993). Saxena et al. (1997) and Saxena and Yu (1998) have verified this model prediction in the southeastern US by finding the existence of aerosol cooling in the southeastern US in the temperature records of the surface air during 1949–1994. The direct aerosol effect refers to scattering and absorption of radiation by the aerosol particles themselves (Charlson et al., 1991; Penner et al., 1994; Kiehl and Briegleb, 1993; IPCC, 1995; Saxena and Yu, 1998). The conclusion of IPCC (1995) is that global mean direct forcing resulting from anthropogenic sulfate may range from -0.25 to $-0.9\,W\,m^{-2}$, with substantial uncertainty; and biomass burning aerosol forcing may range from -0.05 to $-0.6\,W\,m^{-2}$. The low confidence in the estimates of aerosol radiative forcing is due to highly non-uniform compositional, spatial, and

*Corresponding author. Tel.: +1-919-613-8027; fax: +1-919-684-8741.
E-mail address: syu2@duke.edu (S. Yu).

1352-2310/01/$ - see front matter
PII: S1352-2310(01)00187-X

temporal distributions of tropospheric aerosol on regional scales owing to their heterogeneous sources and short lifetimes (Schwartz and Andreae, 1996). The shortwave absorption in Earth's atmosphere due to the absorbing aerosols is also one of the least quantified properties of the climate system (Zender et al., 1997). The comparison of signals of regional aerosol-induced radiative forcing in eastern China and the southeastern US indicates that the high concentration of absorbing aerosol over eastern China was one of the major reasons for the warming trend during 1951–1994 (Yu et al., 2001).

To reduce the uncertainty in the climate effect of tropospheric aerosols in the industrial pollution plumes that are transported from the east coast of the US over the Atlantic Ocean, the tropospheric aerosol radiative forcing observational experiment (TARFOX) was carried out on the eastern coast during July 10–31, 1996 (Russell et al., 1999; Redemann et al., 2000). In two case studies, Redemann et al. (2000) found that the instantaneous shortwave aerosol radiative forcing was of the order of $-36\,W\,m^{-2}$ at the top of the atmosphere (TOA) and about $-56\,W\,m^{-2}$ at the surface. However, the TARFOX datasets do not overlap geographically with the southeastern US nor is it of sufficient length to estimate the regional annual average aerosol direct radiative forcing (ADRF). The objectives of this study are to use tropospheric aerosol measurements to estimate the instantaneous and annual mean ADRF at the surface and TOA, and aerosol absorption over the southeastern US with column radiation model (CRM) of the NCAR (National Center for Atmospheric Research) community climate model (CCM3) (Kiehl et al., 1998; Briegleb, 1992). The atmospheric shortwave absorption due to the aerosol layer was determined as the difference between the TOA ADRF and surface ADRF. Since the ADRF is not determined by surface aerosols only but by total aerosols within the atmospheric column, it is very useful to obtain the average aerosol radiative properties for the atmospheric column, for example, through a column experiment. One of our field sites (Mt. Mitchell) is at a remote and elevated location that is influenced by air masses arriving from marine, continental and polluted sectors. It stays frequently in the free troposphere due to decoupling with the surrounding inversion layer. The data sets are considered to be regionally representative of the southeastern US (Yu et al., 2000; Wenny et al., 1998). We also compare our in situ results with the estimates from other global models for the aerosol radiative forcing in the southeastern US.

2. Retrieval of aerosol radiative properties in the southeastern US

A detailed description of the instrumentation, methodology, data quality assurance and quality control of the data has been given by Wenny et al. (1998) and Yu et al. (2000). Here a brief description is presented. The research sites are a mountain top station located on the peak of Mt. Gibbes (35.78°N, 82.29°W, 2006 m MSL) in Mt. Mitchell State Park, and a valley station located adjacent to the Burnett Reservoir near the town of Black Mountain, North Carolina (35.66°N, 82.38°W, 951 m MSL) (for details see Yu et al., 2000). The two sites are separated horizontally by 10 km and vertically by 1 km. The experimental period was from June 1995 to mid-December 1995. The aerosol optical depths (AOD) at the three operational wavelengths (415, 500 and 673 nm) are determined on the basis of the direct components of solar irradiance measured by the multi-filter rotating shadowband radiometer (MFRSR) (Yu et al., 2000). Table 1 lists the mean total AOD and standard deviation as measured from the valley and mountain sites and mean 1-km layer AOD between the two sites as a function of air mass type for cloud-free days during the experimental period. The clear-sky intervals were determined by a full-sky imaging camera. Total 34 cloud-free days of measuremental data were available because of the bad weather (cloud and rain) situation and instrumental problems during the field experiment period. Fig. 1 shows the time series of AOD at 500 nm for cloud-free periods during the experiment. The air masses are classified (Yu et al., 2000) as highly polluted (HP), marine (M) and continental (C) based on the SO_2 and NO_x emission inventory of the US. Environmental Protection Agency. It is clear from Table 1 that the HP air masses exhibit the largest average AOD, compared to M and C air masses at the three operational wavelengths. The mean total AOD at 500 nm at the valley site was 0.68 ± 0.33, 0.29 ± 0.12, and 0.10 ± 0.04 for HP, M, and C air masses, respectively. As mentioned by Yu et al. (2000), there are two reasons that the mean AOD of marine air masses is higher than that of continental air masses at the research site. First, the marine classification for the sampling site does not imply pure marine air, but rather a modified marine air caused by additional influence from continental and polluted sources between the ocean and the site (the shortest distance between the site and the ocean is about 290 km). Second, the AOD is typically very low during winter months (Peterson et al., 1981). In this study period, the majority of the marine air mass cases occurred during September and early October and the majority of continental air mass cases occurred during late October and November. Overall, the ratios of mean 1-km layer AOD to total mean AOD from the valley site for HP air mass were 73%, 73% and 79% for 415, 500 and 673 nm, respectively. This indicates that the major portion of atmospheric aerosols at our sites, which make an important contribution to the AOD, is located in the lowest 1-km boundary layer of the troposphere. This is in reasonable agreement with that of Hegg et al. (1997),

Table 1
Mean total optical depth, and their standard deviation at 415, 500 and 673 nm as measured at the valley and mountain sites. The data for the intervening layer were obtained from the difference between the two sites. The sites were influenced by highly polluted (HP), continental (C) and marine (M) air masses. V, M, and L denote the valley, mountain and the intervening layer, respectively

Air mass	τ_V at the valley site			τ_M at the mountain site			τ_L for the intervening layer			Ratio (τ_L/τ_V)		
	V415	V500	V673	M415	M500	M673	L415	L500	L673	415	500	673
HP	0.78 ± 0.41	0.68 ± 0.33	0.51 ± 0.22	0.22 ± 0.14	0.19 ± 0.12	0.12 ± 0.07	0.56 ± 0.28	0.50 ± 0.25	0.40 ± 0.20	0.73 ± 0.12	0.73 ± 0.15	0.79 ± 0.17
M	0.36 ± 0.25	0.29 ± 0.19	0.19 ± 0.12	0.13 ± 0.12	0.10 ± 0.09	0.06 ± 0.05	0.23 ± 0.13	0.20 ± 0.11	0.14 ± 0.09	0.69 ± 0.14	0.71 ± 0.15	0.73 ± 0.14
C	0.11 ± 0.07	0.10 ± 0.04	0.07 ± 0.02	0.04 ± 0.02	0.03 ± 0.01	0.03 ± 0.01	0.07 ± 0.04	0.07 ± 0.03	0.04 ± 0.02	0.62 ± 0.12	0.68 ± 0.09	0.51 ± 0.25

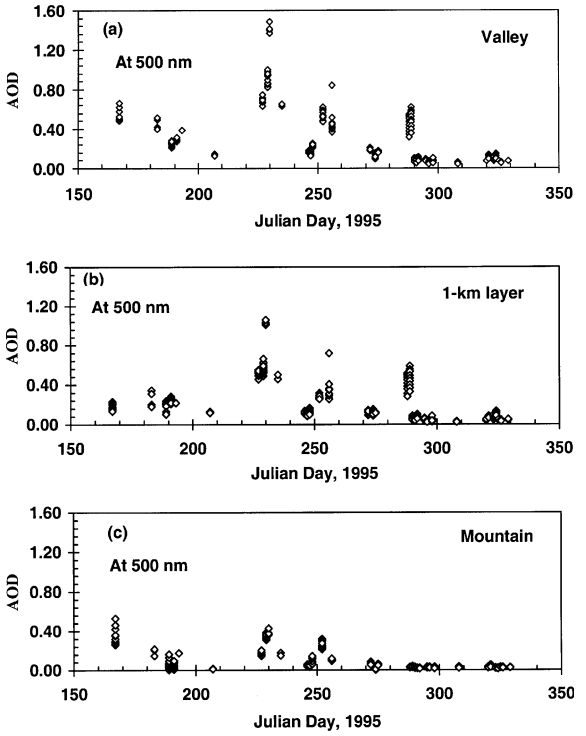

Fig. 1. The time series of aerosol optical depth (AOD) at 500 nm at valley site (A), for 1-km layer between valley and mountain sites (B), and at mountain site (C) for cloud-free period during the experiment from June to mid-December 1995.

who found that AOD for the lowest 4 km of the troposphere constituted over 90% of the total column AOD off the mid-Atlantic coast of the US.

Table 2 lists the experimental results of AOD, and retrieved columnar lognormal size distribution (number concentration (N), number median radius (geometric mean radius, r_g) and geometric standard deviation (σ_g)) by the search-graph method. Table 2 also lists the aerosol radiative properties (imaginary part, asymmetry factor and singe scattering albedo (ϖ)) and ground albedo obtained by using a procedure involving a Mie code and a radiative transfer code in conjunction with the retrieved aerosol size distribution, AOD, and diffuse-direct ratio (DDR) (Yu et al., 2000). A detailed description of the search-graph method and the procedure has been given by Yu et al. (2000). Table 2 shows that N, r_g and σ_g are in the range of 12 to 6000 cm^{-3}, 0.03 to 0.54 μm and 1.12 to 2.95, respectively. The asymmetry factors at 500 nm are in the range of 0.61 to 0.77. ϖ was in the range of 0.72 to 0.97 and the imaginary part of refractive index was in the range of 0.005 to 0.051. Reported values of ϖ in the scientific literature show ϖ to be 1.0 for sulfate and pure marine aerosols and range from 0.5 to 0.9 for desert dust and

Table 2
The measured optical depth (τ) (at 415, 500, 673 nm), columnar size distribution inferred by the search-graph-method, single scattering albedo (ω), asymmetry factor, refractive index, zenith angle, air mass types and instantaneous aerosol direct radiative forcing (ADRF) at the top of the atmosphere (TOA ADRF) and surface (Sfc ADRF) calculated by CRM model. The atmospheric absorption was calculated as the difference between TOA ADRF and Sfc ADRF

				τ measured			Search-graph-method						ADRF ($W m^{-2}$)		
Day (1995)	Time (EST)	Zenith angle	Air mass	415	500	673	Ng (cm^{-3})	rg (μm)	σ_g	g_{500}	ω_{500}	Refractive index	At Sfc	At TOA	Absorption
189(7/8)	8:00	59.2	C	0.33	0.28	0.18	1.70E+02	0.17	1.35	0.74	0.91	1.50-0.017i[a]	−30.2	−10.9	19.3
189(7/8)	8:26	53.9	C	0.3	0.25	0.16	8.40E+01	0.23	1.12	0.76	0.92	1.50-0.017i[a]	−26.8	−8.7	18.1
191(7/10)	8:02	58.9	C	0.33	0.27	0.17	3.30E+02	0.13	1.5	0.73	0.91	1.50-0.017i[a]	−29.7	−10.7	19.0
246(9/3)	8:59	55.4	C	0.21	0.16	0.1	5.40E+02	0.08	1.68	0.67	0.92	1.50-0.015i	−17.5	−6.8	10.7
246(9/3)	9:53	45.3	C	0.23	0.18	0.11	6.70E+02	0.08	1.72	0.7	0.97	1.50-0.005i	−14.3	−9.0	5.3
247(9/4)	8:09	65.5	C	0.18	0.13	0.08	2.30E+03	0.04	2	0.64	0.86	1.50-0.020i	−16.6	−6.0	10.6
247(9/4)	9:01	55.2	C	0.17	0.14	0.08	1.60E+03	0.04	1.94	0.65	0.82	1.50-0.031i	−17.2	−2.0	15.2
247(9/4)	9:28	50.2	C	0.19	0.15	0.09	6.20E+02	0.07	1.74	0.66	0.82	1.50-0.031i	−21.7	−1.9	19.8
256(9/13)	9:10	55.7	C	0.47	0.4	0.27	4.40E+02	0.12	1.57	0.72	0.91	1.50-0.017i[a]	−45.1	−13.4	31.7
256(9/13)	9:52	48.2	C	0.45	0.38	0.25	3.80E+02	0.13	1.55	0.71	0.83	1.50-0.017i[a]	−43.1	−10.8	32.3
290(10/17)	10:00	56.9	C	0.08	0.07	0.07	7.20E+01	0.08	2.25	0.72	0.81	1.50-0.027i[a]	−15.2	−0.5	14.7
290(10/17)	10:40	51.7	C	0.08	0.08	0.08	3.20E+01	0.17	1.77	0.73	0.84	1.50-0.027i[a]	−17.2	−0.1	17.1
295(10/22)	9:50	59.8	C	0.07	0.07	0.06	5.20E+01	0.13	1.8	0.71	0.83	1.50-0.027i[a]	−13.4	−1.7	11.7
295(10/22)	10:30	54.4	C	0.08	0.08	0.06	2.40E+01	0.21	1.48	0.73	0.85	1.50-0.027i[a]	−15.3	−1.4	13.9
296(10/23)	12:42	47.3	C	0.07	0.07	0.06	2.40E+01	0.19	1.61	0.72	0.82	1.50-0.027i[a]	−14	−0.2	13.8
296(10/23)	13:54	51.1	C	0.07	0.07	0.06	4.40E+01	0.1	2.13	0.73	0.75	1.50-0.027i[a]	−15.5	0.5	16.0
298(10/25)	8:36	72.7	C	0.06	0.05	0.05	5.00E+01	0.05	2.95	0.76	0.85	1.50-0.027i[a]	−12.5	−0.7	11.8
298(10/25)	11:09	51.3	C	0.08	0.08	0.07	1.90E+01	0.23	1.47	0.73	0.78	1.50-0.027i[a]	−16.3	−0.7	15.6
308(11/4)	8:48	72.9	C	0.04	0.04	0.04	1.20E+01	0.22	1.47	0.75	0.72	1.50-0.050i[a]	−9.2	−0.6	8.6
320(11/16)	9:06	72.5	C	0.08	0.07	0.06	3.00E+02	0.03	2.7	0.73	0.8	1.50-0.050i[a]	−16.3	−0.3	16.0
320(11/16)	11:38	55.6	C	0.07	0.07	0.06	9.60E+00	0.32	1.15	0.77	0.74	1.50-0.050i[a]	−20.4	1.9	22.3
321(11/17)	10:27	61.8	C	0.14	0.12	0.09	3.20E+02	0.07	1.96	0.69	0.74	1.50-0.051i	−25.5	0.3	25.8
321(11/17)	10:58	58.6	C	0.15	0.13	0.09	1.50E+02	0.11	1.71	0.7	0.74	1.50-0.051i	−27.1	0.7	27.8
321(11/17)	11:45	55.5	C	0.16	0.14	0.1	1.40E+02	0.12	1.68	0.71	0.76	1.50-0.049i	−29.1	1.3	30.4
325(11/21)	9:52	66.8	C	0.08	0.08	0.06	9.20E+01	0.09	1.94	0.71	0.76	1.50-0.050i[a]	−17.9	−0.4	17.5
326(11/22)	10:16	64	C	0.06	0.06	0.05	1.60E+01	0.23	1.45	0.74	0.78	1.50-0.050i[a]	−15.5	0.2	15.7
326(11/22)	10:42	61.2	C	0.07	0.07	0.06	1.60E+01	0.22	1.48	0.75	0.78	1.50-0.050i[a]	−17.7	0.7	18.4
329(11/25)	9:18	72.3	C	0.08	0.08	0.06	5.60E+01	0.12	1.85	0.73	0.76	1.50-0.050i[a]	−17.7	−1	16.7
248(9/5)	10:58	35.5	M	0.3	0.23	0.14	1.10E+03	0.07	1.74	0.61	0.9	1.50-0.017i[a]	−24.3	−4.2	20.1
272(9/29)	8:32	66.9	M	0.25	0.19	0.12	6.00E+03	0.03	2.13	0.63	0.9	1.50-0.017i	−23.1	−9.5	13.6
272(9/29)	8:59	61.9	M	0.24	0.18	0.11	4.10E+03	0.03	2.11	0.69	0.97	1.50-0.010i	−19.2	−10.4	8.8
274(10/1)	8:21	69.6	M	0.12	0.1	0.07	5.80E+02	0.04	2.26	0.67	0.86	1.50-0.020i	−14.6	−5	9.6
274(10/1)	9:01	62.1	M	0.11	0.09	0.07	5.30E+02	0.04	2.37	0.68	0.76	1.50-0.049i	−20.2	0.6	20.8
274(10/1)	9:15	59.6	M	0.11	0.1	0.08	2.00E+02	0.07	2.01	0.68	0.76	1.50-0.049i	−21.4	0.7	22.1
275(10/2)	9:32	56.9	M	0.2	0.16	0.11	1.50E+03	0.04	2.2	0.67	0.98	1.50-0.006i	−16.7	−10.3	6.4
275(10/2)	10:06	51.5	M	0.21	0.18	0.12	6.70E+02	0.06	1.97	0.67	0.97	1.50-0.010i	−19.6	0.4	20.0

Table 2 (*continued*)

Day (1995)	Time (EST)	Zenith angle	Air mass	τ measured			Search-graph-method			g_{500}	ω_{500}	Refractive index	ADRF ($W\,m^{-2}$)		
				415	500	673	Ng (cm^{-3})	rg (μm)	σ_g				At Sfc	At TOA	Absorption
183(7/2)	8:22	54.8	HP	0.57	0.5	0.33	3.60E+02	0.18	1.38	0.72	0.91	1.50-0.017i[a]	−55.3	−16.6	38.7
227(8/15)	8:07	62.1	HP	0.83	0.68	0.43	8.40E+02	0.13	1.52	0.69	0.9	1.50-0.017i[a]	−69.1	−24.8	44.3
227(8/15)	9:50	41.6	HP	0.87	0.71	0.45	5.90E+02	0.15	1.44	0.7	0.91	1.50-0.017i[a]	−73	−14.5	58.5
229(8/17)	9:12	49.3	HP	1.06	0.9	0.59	5.60E+02	0.17	1.4	0.71	0.91	1.50-0.017i[a]	−93.9	−23	70.9
229(8/17)	10:31	34.6	HP	0.99	0.84	0.54	4.80E+02	0.18	1.37	0.71	0.92	1.50-0.017i[a]	−87.4	−11.7	75.7
235(8/23)	9:18	49.3	HP	0.76	0.64	0.41	5.80E+02	0.14	1.48	0.69	0.91	1.50-0.017i[a]	−67.6	−17.6	50.0
252(9/9)	9:19	53	HP	0.81	0.62	0.36	3.00E+03	0.07	1.71	0.64	0.9	1.50-0.017i[a]	−64.8	−19.7	45.1
288(10/15)	11:00	48.8	HP	0.53	0.55	0.68	4.00E+01	0.53	1.28	0.65	0.82	1.50-0.027i[a]	−156.5	20.3	176.8
289(10/16)	8:24	72.7	HP	0.35	0.36	0.42	2.40E+01	0.54	1.36	0.65	0.84	1.50-0.027i[a]	−83.4	−2.5	80.9
289(10/16)	9:40	59.7	HP	0.51	0.52	0.64	3.60E+01	0.54	1.3	0.64	0.84	1.50-0.027i[a]	−142.3	11.4	153.7

[a] The refractive index was obtained by averaging available results (see the text for explanation).

soot aerosols (Lacis and Mishchenko, 1995). Wenny et al. (1998) reported that ϖ at 312 nm varied from 0.75 to 0.93 for aerosols at our research site. Russell et al. (1999) found that the estimated column single scattering albedos for the ambient TARFOX aerosol was ~0.9 at 550 nm. The values of ϖ from this study are consistent with these values given by other authors. Lacis and Mishchenko (1995) showed that the asymmetry factor of soot and large desert aerosols was about 0.9, but for sulfate, marine and smaller dust aerosols the asymmetry factor ranges from 0.65 to 0.8. The values of asymmetry factor reported here are close to those for sulfate, marine and smaller dust aerosols. Since the size distribution was inferred from the total AOD, the aerosol radiative properties derived by this method represent a weighted average over the entire column. Yu et al. (2000) found that ground albedo is 0.19 ± 0.10 at our research site. The mean ground albedo (0.19) was used in the calculation of this study.

3. Calculation of aerosol direct radiative forcing and aerosol absorption

The NCAR CCM3 CRM (Kiehl et al., 1998; Briegleb, 1992) is used to estimate the TOA and surface ADRF and aerosol absorption for the measurement sites. The CCM3 CRM uses an δ-Eddington approximation with 19 spectral intervals (7 for O_3, 2 for the visible, 7 for H_2O, and 3 for CO_2) spanning the solar spectrum from 0.2 to 5.0 μm. A detailed description of all the physical and numerical methods used in CCM3 CRM is given in Kiehl et al. (1998) and Briegleb (1992). The atmospheric initial conditions of Kiehl and Briegleb (1993) for mid-latitude summer vertical profiles of temperature, pressure, ozone and H_2O vapor mixing ratios were used in the CRM. The mass extinction coefficient, single scattering albedo and asymmetry factor at 19 spectral interval wavelengths calculated by a Mie code with the retrieved columnar size distribution and refractive index, and ground albedo (0.19) were input into the CRM. The density of aerosol particles was assumed to be $1.86\,g\,cm^{-3}$. The ADRF is obtained as the difference in shortwave net radiative fluxes at the TOA (or at the surface) between CRM simulations with and without aerosol mass loading. We also infer the atmospheric absorption due to boundary layer aerosols as the difference between the TOA ADRF and surface ADRF.

Table 2 lists the examples of the instantaneous ADRF for each cloud-free time during the experiment. The zenith angle, air mass types, AOD at the three wavelengths, size distribution, retrieved aerosol radiative properties and refractive indices are listed in Table 2. Hansen et al. (1997) indicated that the ADRF is very sensitive to single scattering albedo (or imaginary part of refractive index). Unfortunately, it is very difficult to

retrieve mean single scattering albedo for the whole atmospheric column. As mentioned by Yu et al. (2000), our DDR method can only have solutions for the cases whose AOD at 500 nm was between 0.1 and 0.3. The averages of the imaginary part of refractive index for September, October and November are -0.017 ± 0.009, -0.027 ± 0.021, -0.050 ± 0.001 on the basis of available results in Table 2. The values of -0.017, -0.027 and -0.050 were used for cases for which imaginary part of refractive index is not available, between July and September, in October and in November, respectively, as indicated in Table 2. Since entirely cloud-free days were very rare, we assume that the aerosol radiative properties obtained at one cloud-free time were constant to study the diurnal variation of instantaneous cloud-free ADRF. Fig. 2 shows the diurnal variations of instantaneous surface and TOA ADRF for C, M, and HP air masses, calculated on the basis of measurements at Julian Day 321 (11/17/1995, 10:27), 272 (9/29/1995, 8:59) and 227 (8/15/1995, 9:50) (see Table 2). The diurnal behavior of the TOA aerosol direct radiative forcing (ADRF) is determined by the changing ratio of aerosol forward-scattered radiation (scattering angle less than 90°) to aerosol up-scattered radiation (scattering up to space rather than down to surface) as the zenith angle changes (Wiscombe and Grams, 1976). When the sun is closer to the horizon much (up to half) of the forward-scattered sunlight corresponds to up-scattered radiation that is reflected back to space and thus cools the climate system (hence ADRF minima (more negative) at twilight). When the sun is overhead, the forward-scattered solar radiation coincides with the down-scattered radiation, i.e., it penetrates the aerosol layer where it may be absorbed by the absorbing aerosols or by the surface, warming the climate system (hence ADRF maxima (less negative) at noon). These results are in agreement with those of Russell et al. (1997). Fig. 2 also indicates that the TOA ADRF is much smaller than surface ADRF during the daytime (from sunrise to sunset), especially for highly absorbing aerosol (small single scattering albedo) and at the mid-day peak of incident sunlight. This is consistent with the finding of Satheesh and Ramananthan (2000) who reported the large difference in tropical aerosol forcing at TOA and the Earth's surface due largely to solar absorption by carbonaceous aerosol.

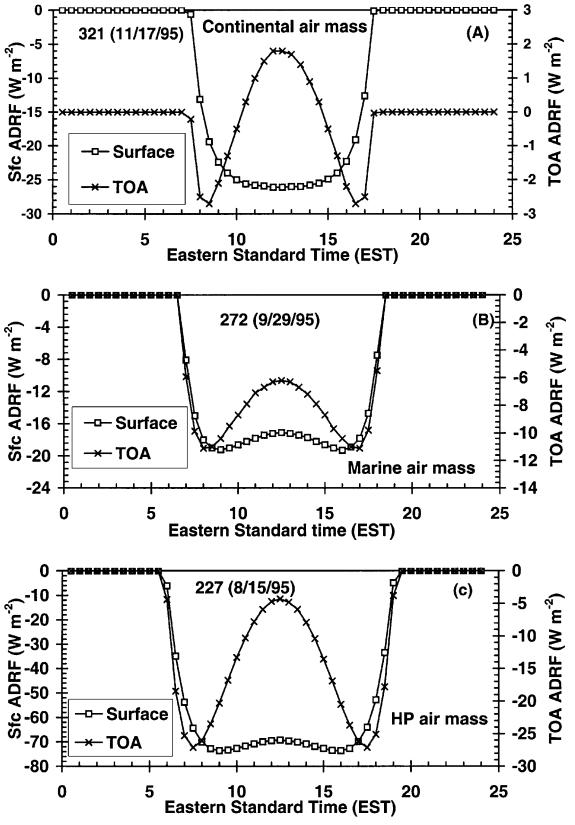

Fig. 2. The instantaneous aerosol direct radiative forcing (ADRF) at the top of the atmosphere (TOA) and the Sfc (surface) as a function of local time for three cases on the basis of the aerosol measurements on 11/17/1995 10:27 (continental air mass) (A), 9/29/1995 8:59 (marine air mass) (B), and 8/15/1995 9:50 (highly polluted air mass) (C). The calculations assume that the aerosol radiative properties measured are constant for the whole day. 'Sfc', and 'TOA' represent instantaneous aerosol forcing at the surface and at the TOA, respectively.

Table 2 shows that the instantaneous TOA ADRF ranges from +20.3 to –24.8, +1.3 to −10.4, and +1.9 to –13.4 W m^{-2} for HP, M, and C air masses, respectively. The instantaneous surface ADRF ranges from –55.3 to −156.5, −16.7 to −24.3, and −9.2 to −30.2 W m^{-2} for HP, M, and C air masses, respectively. The atmospheric aerosol absorption ranges from 5.3 to 176.8 W m^2, and is always positive. Clearly, the difference between ADRF at surface and TOA are very large, especially for highly absorbing aerosols. The inclusion of absorbing aerosols makes the ADRF at TOA less negative while making the ADRF at the surface more negative. This is in agreement with the results of Hignett et al. (1999). Fig. 3 shows the surface and TOA ADRF, and absorption as functions of aerosol optical depth and single scattering albedo. As can be seen, the surface ADRF was generally more sensitive to AOD and single scattering albedo than TOA ADRF. Note that the zenith angle (or local time) is also an important factor for ADRF as indicated in Fig. 2. Figs. 3a and b also show that both surface and TOA ADRFs are more sensitive to the AOD than single scattering albedo on the basis of the correlation coefficients. The small single scattering albedo (more absorbing) and large optical depth will greatly increase the heating rate of the atmosphere due to aerosols as indicated in Fig. 3 and

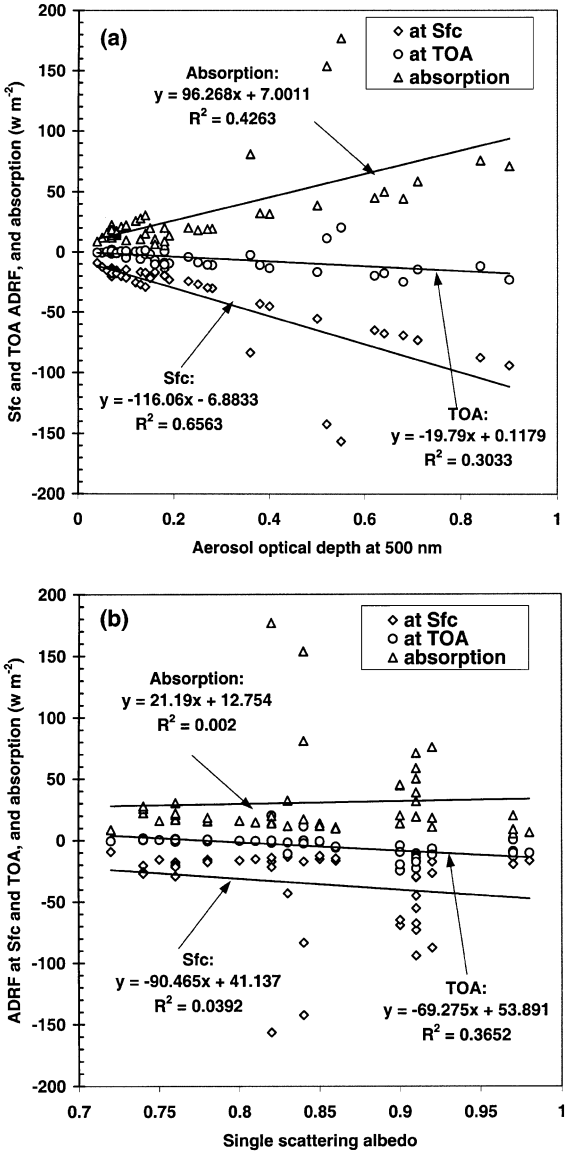

Fig. 3. The aerosol direct radiative forcing (ADRF) at the TOA, surface (Sfc) and atmospheric absorption due to aerosol as functions of aerosol optical depth (a) and single scattering albedo (b) on the basis of the results of Table 2.

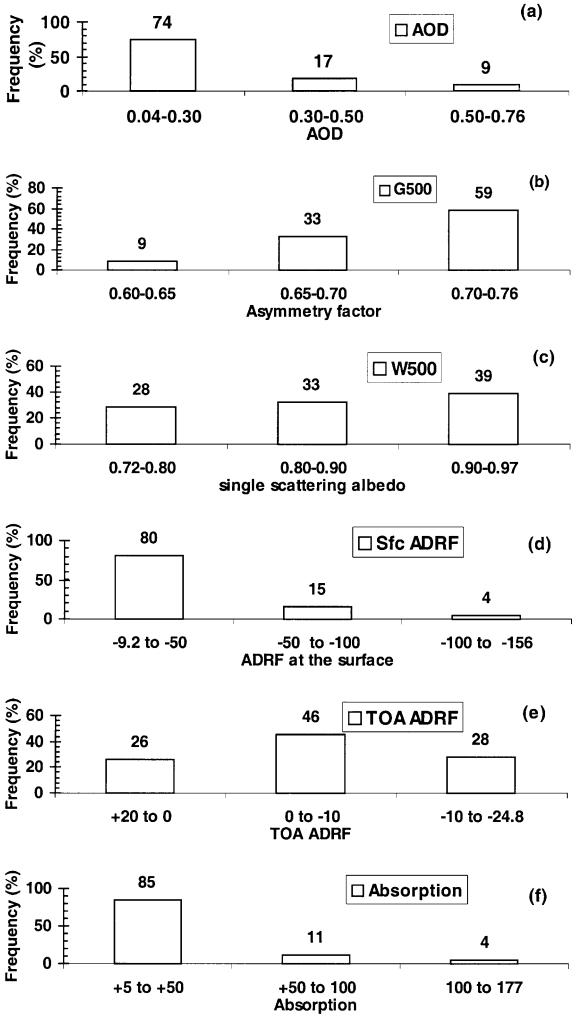

Fig. 4. Statistical summaries of aerosol optical depth (a), asymmetry factor (b), single scattering albedo (c), Sfc ADRF ($W m^{-2}$) (d), TOA ADRF ($W m^{-2}$) (e) and absorption ($W m^{-2}$) (f) for the absolute magnitude ranges and their frequencies of occurrences on the basis of the results of Table 2.

Table 2. Fig. 4 shows the statistical summaries of ranges of the AOD, asymmetry factor, single scattering albedo, surface and TOA ADRF, and absorption with their frequencies of occurrences on the basis of Table 2. As can be seen, the most frequencies of occurrences for AOD, surface ADRF, TOA ADRF and absorption are in the ranges of 0.04 to 0.30, -9.2 to $-50\,W m^{-2}$, 0 to $-10\,W m^{-2}$, and $+5$ to $+50\,W m^{-2}$, respectively.

A sensitivity test was performed by calculating the ADRF difference between the case with our aerosol radiative properties and that with the sulfate optical properties of Kiehl and Briegleb (1993), keeping the AOD same. It is found that the instantaneous surface ADRF is $-27.2\,W m^{-2}$ on the basis of measurement of aerosol radiative properties at 10:58 AM, 11/17/1995, while the surface ADRF is $-10.0\,W m^{-2}$ on the basis of sulfate aerosol radiative properties of Kiehl and Briegleb (1993). The surface ADRF from this study is much higher. This is reasonable because the aerosol of this study is total aerosol and the imaginary part of refractive index is also considered.

To estimate the 24 h and annual average ADRF for different air mass types for the whole year, it is ideal to

Table 3
Comparison of aerosol direct radiative forcing (ADRF) at the top of the atmosphere (TOA) and surface in the southeastern US and eastern US

Aerosols	Method	ADRF at TOA ($W m^{-2}$)	ADRF at surface ($W m^{-2}$)	Regions	Author
Total aerosol(marine)	Measurement and CCM3 CRM	-3 ± 2 (with cloud)[a]	-5 ± 3 (with cloud)[a]	SE US	This work
Total aerosol (continental)	Measurement and CCM3 CRM	-0.05 ± 0.02 (with cloud)[a]	-3 ± 1 (with cloud)[a]	SE US	This work
Total aerosol(polluted)	Measurement and CCM3 CRM	-3 ± 2 (with cloud)[a]	-13 ± 6 (with cloud)[a]	SE US	This work
Total aerosol (average)	Measurement and CCM3 CRM	-2 ± 1 (with cloud)[a]	-7 ± 2 (with cloud)[a]	SE US	This work
Total aerosol(marine)	Measurement and CCM3 CRM	-7 ± 4 (no cloud)[a]	-13 ± 8 (no cloud)[a]	SE US	This work
Total aerosol (continental)	Measurement and CCM3 CRM	-0.14 ± 0.05 (no cloud)[a]	-8 ± 3 (no cloud)[a]	SE US	This work
Total aerosol(polluted)	Measurement and CCM3 CRM	-8 ± 4 (no cloud)[a]	-33 ± 16 (no cloud)[a]	SE US	This work
Total aerosol (average)	Measurement and CCM3 CRM	-5 ± 3 (no cloud)[a]	-17 ± 6 (no cloud)[a]	SE US	This work
Total aerosol (marine)	Box model	-9		SE US	Saxena and Yu (1998)
Total aerosol (continental)	Box model	-3		SE US	Saxena and Yu (1998)
Total aerosol (polluted)	Box model	-21		SE US	Saxena and Yu (1998)
Sulfate	GCM model	~ -2		SE US	Boucher and Anderson (1995)
Anthropogenic sulfate	Box model	-2		E US	Charlson et al. (1991)
Anthropogenic sulfate	3-D chemical and CCM3 CRM	-3		E US	Kiehl and Briegleb (1993)
Sulfate	AGCM model	~ -0.5 to ~ -1.5		E US	IPCC (1995)
Anthropogenic sulfate		-3		E US	Taylor and Penner (1994)
Total aerosol	radiative transfer model	-9		E US	Russell et al. (1997)
Total aerosol	radiative transfer model	-8 to ~ -50 (no cloud)[a]		E US	Bergstrom and Russell (1999)
Anthropogenic sulfate	slow oxidation rate case	-2		E US	Langner and Rodhe (1991)
Anthropogenic sulfate	chemical model	-5		E US	Kiehl and Rodhe (1995)
Antropogenic aerosol	internal mixture	-1.5		E US	Haywood and Shine (1995)
Sulfate + BC	1-D radiative transfer model	-2 to -3		E US	Schult et al. (1997)
Sulfate	GCM model	-5		E US	Haywood and Ramaswamy (1998)
Sulfate + BC	GCM model	-3		E US	Haywood and Ramaswamy (1998)

[a] "No cloud" means cloud-free 24-h average, "with cloud" means that the fractional coverage of clouds is assumed to be 0.61.

measure the aerosol radiative properties and calculate the aerosol forcing for each air mass and then average them during the cloud-free period for the whole year. Unfortunately, the information is very scarce. In this study, we select the typical aerosol radiative properties (mass extinction coefficient, single scattering albedo, asymmetry factor) of 321 (11/17/1995, 10:27 EST, C air mass), 272 (9/29/1995, 8:59 EST, M air mass) and 227 (8/15/1995, 9:50 EST, HP air mass) as representatives for the C, M, and HP air masses, respectively. These three cases were selected because their AOD was close to the mean AOD of corresponding air masses and most of continental, marine, and polluted air masses occurred during winter, fall and summer seasons, respectively as shown in Tables 1 and 2. Then, the mean optical depths in Table 1 for three air mass types are used in the calculation. It was found that the mean cloud-free 24-h ADRF at the TOA (and at the surface) for HP, M, and C air masses was estimated to be -8 ± 4 (-33 ± 16), -7 ± 4 (-13 ± 8), and -0.14 ± 0.05 (-8 ± 3) $W m^{-2}$, respectively, as listed in Table 3. To assess the annual average ADRF in the southeastern US, the relative contributions of three air masses are needed. On the basis of back trajectory analysis of air masses from June 1996 to October 1996, and from March 1997 to June 1997, Bahrmann and Saxena (1998) found that the percentages of air masses influencing our research site were 43.2, 22.4 and 34.4% for C, M, and HP masses, respectively. Using these percentages, the annual cloud-free, 24-h mean ADRF at the TOA (and at the surface) was estimated to be -5 ± 3 (-17 ± 6) $W m^{-2}$. If the mean fraction of the area with clear sky condition in the southeastern US is assumed to be 0.39, which is the globally average clear sky condition (Charlson et al., 1991), the mean ADRF at the TOA (and at the surface) will be -3.2 ± 1.5 (13 ± 6), -2.7 ± 1.5 (-5 ± 3), and -0.05 ± 0.02 (-3 ± 1) $W m^{-2}$ for HP, M, and C air masses, respectively. The annual mean ADRF at the TOA (and at the surface) is -2 ± 1 (-7 ± 2) $W m^{-2}$. Note that we assume that the ADRF is zero when clouds are present. So our estimate of annual mean ADRF is a lower bound. The annual mean atmospheric absorption due to aerosol layer will be $5 \pm 3 W m^2$.

Table 3 lists the comparison of our estimates of ADRF with those of other investigators for the southeastern US or eastern US. The methods used by each author are also listed in Table 3. As can be seen, box models, GCM and column radiation models have been used to estimate the ADRF on the basis of the actual measurements or chemical simulation. The estimates of ADRF in the eastern US (or southeastern US) have a large variation because of different assumptions in each model and relative uncertainty of aerosol radiative properties. Our annual estimated TOA ADRF ($-2 \pm 1 W m^{-2}$) was close to those of Boucher and Anderson (1995), Schult et al. (1997) and Haywood and Ramaswamy (1998), but a little lower than those of Bergstrom and Russell (1999), Kiehl and Rodhe (1995). Bergstrom and Russell (1999) show that cloud-free, 24-h average ADRF is $-9 W m^{-2}$ near the eastern US coast in summer. Since our calculations are for total aerosols (anthropogenic + natural) and for whole aerosol components (sulfate + organic), our estimated ADRF is consistent with the reported values. The major portion of atmospheric aerosol at our sites is located in the lowest 1-km boundary layer of the troposphere where it exerts a negligible longwave forcing. Thus we make the approximation that ADRF is due to shortwave forcing alone. It is noteworthy that although there was large negative ADRF at the surface, the atmospheric heating rate due to aerosols is large, especially for high polluted absorbing aerosols. As pointed out by Ackerman et al. (2000) and Hansen et al. (1997), absorbing aerosols were more effective than their radiative forcing due to their cloud-burning effects. Further observations on absorbing aerosols are obviously needed.

4. Conclusion

Using a column radiation model, the instantaneous and cloud-free 24-h average ADRF at both TOA and surface for C, M, and HP air masses in the southeastern US was estimated on the basis of measurements of aerosol radiative properties. The results show that the annual regional cloud-free mean ADRF at the TOA (and at the surface) is -5 ± 3 (-17 ± 6) $W m^{-2}$. Considering the effect of cloud fraction, we estimate that the annual regional mean ADRF at the TOA (and at the surface) is -2 ± 1 (-7 ± 2) $W m^{-2}$. This estimate of ADRF in the southeastern US is close to those of other investigators (see Table 3) when they considered both sulfate and black carbon. Since our study considers the total aerosol (anthropogenic + natural) instead of anthropogenic and whole aerosol (sulfate + organics) instead of sulfate, our estimated ADRF provide an upper bound on the direct effect of anthropogenic aerosols. This study confirms the existence of a cooling effect (negative forcing) due to the direct effect of aerosol at the surface in the southeastern US as indicated by Saxena and Yu (1998). However, the atmosphere of the troposphere above the ground is still heated with annual mean rate of $5 \pm 3 W m^{-2}$ due to the aerosol layer. Since the aerosol field and composition are inhomogeneous in time and space, and our study also indicates the effect of long-range transport of pollution from other regions, the complexity of this aerosol puzzle seems to grow with each new study as pointed out by Kiehl (1999). Continuity in the long-term monitoring of the aerosol properties, especially for absorbing aerosol, is still crucial in improving the understanding of role of aerosols in the climate change.

Acknowledgements

This research was supported by the NASA's Mission to Planet Earth (MTPE) under Contract No. NAS1-18944 from Langley Research Center, Hampton, VA, and Grant NA76GP0350 from NOAA Office of Global Programs and Subcontract G-35-W62-G2 from Georgia Institute of Technology (Principal grant R 826372-01-0 from EPA). Dr. B.N. Wenny performed the field experiment.

References

Ackerman, A.S., Toon, O.B., Stevens, D.E., Heymsfield, A.J., Ramanathan, V., Welton, E.J., 2000. Reduction of tropical cloudiness by soot. Science 288, 1042–1047.

Bahrmann, C.P., Saxena, V.K., 1998. The influence of air mass history on black carbon concentrations in the southeastern US. Journal of Geophysical Research 103, 23153–23161.

Bergstrom, R.W., Russell, P.B., 1999. Estimation of aersol direct radiative effects over the mid-latitude North Atlantic from satellite and in situ measurements. Geophysical Research Letters 26, 1731–1734.

Boucher, O., Anderson, T.L., 1995. General circulation model assessment of the sensitivity of direct climate forcing by anthropogenic sulfate aerosols to aerosol size and chemistry. Journal of Geophysical Research 100, 26117–26134.

Briegleb, B.P., 1992. Delta-{Eddington} approximation for solar radiation in the NCAR Community Climate Model. Journal of Geophysical Research 97, 7603–7612.

Charlson, R.J., Langner, J., Rodhe, H., Leovy, C.B., Warren, S.G., 1991. Perturbation of the northern hemisphere radiative balance by backscattering from anthropogenic sulfate aerosols. Tellus 43AB, 152–163.

Hansen, J., Lacis, A., Ruedy, R., 1997. Radiative forcing and climate response. Journal of Geophysical Research 102, 6831–6864.

Haywood, J.M., Ramaswamy, V., 1998. Global sensitivity studies of the direct radiative forcing due to anthropogenic sulfate and black carbon aerosol. Journal of Geophysical Research 103, 6043–6058.

Haywood, J.M., Shine, K.P., 1995. The effect of anthropogenic sulfate and soot aerosol on the clear sky planetary radiation budget. Geophysical Research Letters 22, 603–606.

Hegg, D.A., Livingston, J., Hobbs, P.V., Novakov, T., Russell, P., 1997. Chemical apportionment of aerosol column optical depth off the mid-Atlantic coast of the United States. Journal of Geophysical Research 102, 25293–25303.

Hignett, P., Taylor, J.P., Francis, P.N., Glew, M.D., 1999. Comparison of observed and modeled direct aerosol forcing during TARFOX. Journal of Geophysical Research 104, 2279–2287.

IPCC., 1994. Climatic change 1995. In: Houghton, J.T., et al. (Eds.), The Science of Climate Change. Cambridge University Press, Cambridge, UK.

Kiehl, J.T., 1999. Solving the aerosol puzzle. Science 283, 1273–1275.

Kiehl, J.T., Briegleb, B.P., 1993. The relative role of sulfate aerosols and greenhouse gases in climate forcing. Science 260, 311–314.

Kiehl, J.T., Hack, J.J., Bonan, G.B., Boville, B.A., Williamson, D.L., Rasch, P.J., 1998. The national center for atmospheric research community climate model: CCM3. Journal of Climate 11, 1131–1149.

Kiehl, J.T., Rodhe, H., 1995. Modeling geographical and seasonal forcing due to aerosols. In: Charlson, R.J., Heintzenberg, J. (Eds.), Proceedings of the Dahlem Work Shop on Aerosol Forcing of Climate. John Wiley and Sons, Chichester.

Lacis, A., Mishchenko, M.I., 1995. Climate forcing, cloud sensitivity, and climate response: a radiative modeling perspective on atmospheric aerosols. In: Charlson, R.J., Heintzenberg, J. (Eds.), Aerosol Forcing of Climate. Wiley, Chichester, UK.

Langner, J., Rodhe, H., 1991. A global three dimensional sulfur cycle. Journal of Atmospheric Chemistry 13, 225–263.

Penner, J.E., Charlson, R.J., Hales, J.M., Laulainen, N.S., Leifer, R., Novakov, T., Ogren, J., Radke, L.F., Schwartz, S.E., Travis, L., 1994. Quantifying and minimizing uncertainty of climate forcing by anthropogenic aerosols. Bulletin of American Meteorological Society 75, 375–400.

Peterson, J.T., Flowers, E.C., Berri, G.J., Reynolds, C.L., Rudesill, J.H., 1981. Atmospheric turbidity over central North Carolina. Journal of Applied Meteorology 20, 229–241.

Redemann, J., Turco, R.P., Liou, K.N., Hobbs, P.V., Hartley, W.S., Berstrom, R.W., Browell, E.V., Russell, P.B., 2000. Case studies of the vertical structure of the direct shortwave aerosol radiative forcing during TARFOX. Journal of Geophysical Research 105, 9971–9979.

Russell, P.B., Kinne, S.A., Bergstrom, R.W., 1997. Aerosol climate effects: local radiative forcing and column closure experiments. Journal of Geophysical Research 102, 9397–9407.

Russell, P.B., Livingston, J.M., Hignett, P., Kinne, S.A., Wong, J., Chien, A., Bergstrom, R.W., Durkee, P., Hobbs, P.V., 1999. Aerosol-induced radiative flux changes off the United States mid-Atlantic coast: comparison of values calculated from sunphotometer and in situ data with those measured by airborne pyranometer. Journal of Geophysical Research 104, 2289–2307.

Satheesh, S.K., Ramanathan, V., 2000. Large differences in tropical aerosol forcing at the top of the atmosphere and Earth's surface. Nature 405, 60–63.

Saxena, V.K., Yu, S., 1998. Searching for a regional fingerprint of aerosol radiative forcing in the southeastern US. Geophysical Research Letters 25, 2833–2836.

Saxena, V.K., Yu, S., Anderson, J., 1997. Impact of stratospheric volcanic aerosols on climate: evidence for aerosol shortwave and longwave forcing in the Southeastern US. Atmospheric Environment 31, 4211–4221.

Schult, I., Feichter, J., Cooke, W.F., 1997. Effect of black carbon and sulfate aerosols on the global radaition budget. Journal of Geophysical Research 102, 30107–30117.

Schwartz, S.E., Andreae, M.O., 1996. Uncertainty in climate change caused by aerosols. Science 272, 1121–1122.

Taylor, K., Penner, J.E., 1994. Response of the climate system to atmospheric aerosols and greenhouse gases. Nature 369, 734–737.

Wenny, B.N., Schafer, J.S., DeLuisi, J.J., Saxena, V.K., Barnard, W.F., Petropavlovskikh, I.V., Vergamini, A.J., 1998. A study of regional aerosol radiative properties and effects on ultraviolet-β radiation. Journal of Geophysical Research 103, 17083–17097.

Wiscombe, W.J., Grams, G.W., 1976. The backscattered fraction in two-stream approximations. Journal of Atmospheric Science 33, 2440–2451.

Yu, S., Saxena, V.K., Wenny, B.N., DeLuisi, J.J., Yue, G.K., Petropavlovskikh, I.V., 2000. A study of the aerosol radiative properties needed to compute direct aerosol forcing in the southeastern US. Journal of Geophysical Research 105, 24739–24749.

Yu, S., Saxena, V.K., Zhao, Z., 2001. A comparison of signals of the regional aerosol-induced radiative forcing in eastern China and the southeastern US. Geophysical Research Letters 28, 713–716.

Zender, C.S., Bush, B., Pope, S.K., Bucholtz, A., Collins, W.D., Kiehl, J.T., Valero, F.P.J., Vitko, J., 1997. Atmospheric absorption during the atmospheric radiation measurement enhanced shortwave experiment (ARESE). Journal of Geophysical Research 102, 29901–29915.